



Oblate spheroidal droplet evaporation in an acoustic levitator

Belal Al Zaitone

Department of Chemical and Materials Engineering, King Abdulaziz University, Jeddah 21589, Saudi Arabia



ARTICLE INFO

Article history:

Received 17 November 2017

Received in revised form 22 May 2018

Accepted 4 June 2018

Available online 18 June 2018

Keywords:

Evaporation

Single droplet

Acoustic levitation

Oblate spheroid

Modelling

ABSTRACT

The modelling of evaporation in which droplet geometry deviates from sphericity, i.e., oblate spheroid, when the droplet experiences high dynamic stresses or a high Weber number, is important in many applications. The validation of such theoretical models is often difficult to achieve experimentally. The acoustic levitation technique was used to investigate the evaporation of an oblate spheroid for different liquids. Evaporation of oblate droplet at constant aspect ratio is realized through the course of evaporation in the acoustic levitator by continuously adjusting the applied acoustic force on the droplet. A Two-dimensional axisymmetric computational model in oblate coordinate system is presented to predict droplet evaporation driven by the acoustic boundary layer, the model calculates the vapor flux at each grid point on droplet surface. The evaporation follows the d^2 -law and a good agreement between model prediction and experiments is demonstrated. The acoustic levitator allows for the study of the evaporation of freely suspended deformed droplets and validates the theoretical model of oblate droplet evaporation.

© 2018 Elsevier Ltd. All rights reserved.

1. Introduction

The evaporation of droplets is an essential step in various chemical engineering processes, such as spray drying, fuel combustion, the prevention of aircraft icing and nanomaterial fabrication. In these applications, multiple physical phenomena often occur, including droplet atomization, spray transport, droplet-wall interactions, collisions, coalescence, oscillations (including the instabilities of evaporating droplets) and, on the scale of single droplets, heating and subsequent evaporation of a liquid solvent.

Modelling of the diffusion process involved in vaporizing droplets has attracted many researchers. The simplest model for diffusion controlled evaporation was proposed by Maxwell [1]. Maxwell's model addressed stationary state evaporation and assumed that the concentration gradient of the solvent vapor between the droplet surface and the surrounding gaseous medium was the sole driving force behind the vapor's transport. Maxwell's equation ignores the gas convective flow effect, which limits its applicability. Fuchs [1] took Maxwell's model one step further by solving mass diffusion and heat flow simultaneously. Fuchs assumed that heat is transferred due to conduction and neglected the radiation and convection effects. It is worth noting that both models attempted to simulate the steady state evaporation of a non-moving droplet.

In most cases, droplets move relative to the gaseous medium, which results in convective transport of the evaporated solvent.

Film theory [2] introduced the influence of convective flow. An empirical correlation [3,4] was proposed to account for the evaporation of a droplet by forced or natural convection. These correlations are usually written in terms of Sherwood/Nusselt numbers that relate the mass/heat transfer of moving droplets to that of a stationary one.

Abramzon and Sirignano [5] presented a theoretical model based on the concept of film theory. They studied the convective transport induced by droplet motion or the effects of gas blowing and employed the diffusion and thermal boundary layer thickness to compute the convective mass and heat transfer between the droplet's surface and the air stream.

Another implementation of the film theory concept [6] was similar to Abramzon and Sirignano's model but with a modified boundary condition that considers droplets' surface recession during evaporation and Stephan flow, resulting in a generalized form of mass and heat transfer coefficients.

Evaporation of multicomponent liquid droplets was investigated by many researchers [6–9], either using semi-analytical approach [10] or in case of spray evaporation; CFD models [11] were implemented to study different evaporation problems. Brenn et al. [7] developed a computational model based on Abramzon and Sirignano's model to simulate the evaporation of single droplet consisting of up to five liquid components, the influence of various liquid component activities was modeled using the UNIFAC approach. They used an empirical correlation for Sh number found by Ranz and Marshall [3] for convective mass transfer, even though the evaporation is driven by the acoustic boundary layer.

E-mail address: balzaitone@kau.edu.sa

Nomenclature

a	semi-major axis ratio, [m]	x, y, z	cartesian coordinates system
A_{os}	surface area of oblate spheroid, [m ²]	y_s	vapor fraction at the surface, [-]
A_R	aspect ratio = b/a [-]		
b	semi-minor axis ratio, [m]		
C_p	heat capacity, [kJ/(kg·K)]	<i>Greeks</i>	
c_s	sound velocity, [m/s]	ξ, θ and φ	oblate coordinates system
e	oblate spheroid eccentricity, ($e^2 = 1 - A_R^2$)	α	thermal diffusivity, [m ² /s]
f	focal length, [m]	ρ	density [kg/m ³]
h_g	heat transfer coefficient, [W/(m ² ·K)]	λ	heat vaporization of liquid, [kJ/kg]
$h_\xi, h_\theta, h_\varphi$	metric coefficients	\mathfrak{D}_g	diffusion coefficient, [m ² /s]
k_d	heat conductivity of droplet, [W/(m·K)]	ω	angular frequency, [Hz]
L_c	characteristic length, [m]		
L_{major}	equatorial diameter ($L_{major} = 2a$), [m]	<i>Subscripts</i>	
L_{minor}	axial diameter ($L_{minor} = 2b$), [m]	os	Oblate spheroid
Mw	molecular weight, [g/mol]	s	surface of droplet
Nu	Nusselt number, [-]	d	droplet
P^*	vapor pressure, [atm]	g	gas
P_{amt}	ambient gas pressure, [atm]	vap	vapour
Sh	Sherwood number, [-]		
T	temperature, [k]		

Modelling of droplet evaporation was developed primarily for a simplified geometrical shape, i.e., a spherical droplet. Experimental studies showed that droplet geometry may have a significant shape deformation; a droplet moving in a gas medium is prone to dynamic stresses on the droplet's surface [12]; while the gas's dynamic stress forces the droplet to deform, the surface tension tends to retain the droplet's surface to an equilibrium surface energy which leads to a spherical shape [13]. At a Weber number much greater than unity, droplet shape deviates from sphericity [14], any change in liquid surface tension might cause the droplet shape to oscillate [15].

Many monographs have studied the heating of spheroid droplets in terms of the heat transfer coefficient. They addressed the energy and Navier-Stokes equations that describe the flow past the spheroid [16–19]. Spheroidal droplet evaporation has been investigated theoretically for oscillating spheroidal liquid drops [20]. A general 1-D mathematical approach was developed [21] and results in an analytical solution to steady-state evaporation from spheroidal droplets (oblate, prolate and triaxial ellipsoids). A theoretical study was conducted on deformed droplets under forced convection evaporation [22]; it sought to obtain an algebraic solution for the evaporation rate of an oblate droplet. The researchers validated their model for the spherical case only and assumed an empirical correlation for Sherwood/Nusselt numbers based on geometrical analysis instead of solving the Navier-Stokes equation that describes the flow around the oblate spheroid.

In recent work from our laboratory, Al Zaitone [23] investigated theoretically the evaporation of an oblate liquid droplet. The evaporation is driven by the forced convection of air stream past the droplet, the governing equations of energy, mass and momentum were solved numerically. The influence of droplet geometry i.e. aspect ratio on the resulting profiles of Sherwood/Nusselt numbers on droplet were calculated. Al Zaitone presented a quantitative analysis of the shape factor effect on evaporation rate of spheroidal droplets versus spherical droplets, the study shows that the maximum deviation of evaporation rate occurs as oblateness of the spheroid approaches disk-like shape for the same equivalent volume of spherical droplets.

Experimental observations revealed that spheroids are a good approximation of non-spherical particles [24]. A sphere is a special

case of generalized spheroidal geometry; for example, most aerosols are not spherical in nature [25]. A recent review [26] shows that elongated particles are more efficient at enhancing targeted drug delivery, as they can easily pass through cell membranes.

In most studies involving the evaporation of spheroidal droplets, only a theoretical analysis has been presented. In sprays, droplets might deform due to the high aerodynamic forces exerted, which leads to droplet disintegration. Such phenomena happen in a very short time and it is difficult to observe this evaporation experimentally. The validation of theoretical models through experimental results is important.

Successful modelling tools for understanding transport processes are highly related to an accurate description of the drop's geometry. Therefore, the objective of the present study is to experimentally investigate the evaporation of oblate droplets using the acoustic levitation technique. The unique feature of acoustic levitation – holding up freely suspended droplets in the air – is used to generate an oblate droplet of a predefined droplet geometry, i.e., the aspect ratio during the evaporation process which allows the theoretical model predictions for an oblate spheroidal coordinate to be validated with experiments. The mathematical model of deformed droplet evaporation is first presented, then the acoustic levitator is described in the experimental method section followed by an analysis of acoustic field influence on evaporation of single droplet. Experimental results of deformed droplet evaporation at constant aspect ratio is discussed. The mathematical model is verified using experimental data acquired with an acoustic levitator, and a further study of deformed droplet evaporation at various aspect ratio from the computational model is discussed, finally the conclusions of the present work is drawn in the last section.

2. Oblate droplet evaporation model

Oblate spheroids droplets are formed by revolving an ellipse around its minor axis, the oblate orthogonal coordinates shown in Fig. 1 is related to the cartesian coordinates [28]:

$$\begin{aligned} X &= f \cdot \cosh \xi \cdot \sin \theta \cdot \cos \varphi \\ Y &= f \cdot \cosh \xi \cdot \sin \theta \cdot \sin \varphi \\ Z &= f \cdot \sinh \xi \cdot \cos \theta \end{aligned} \quad (1)$$

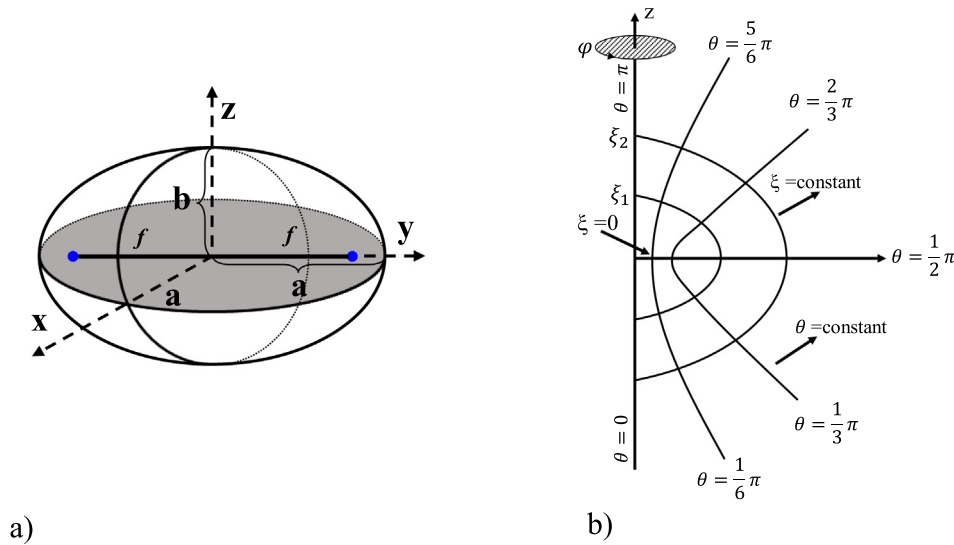


Fig. 1. (a) 3-D oblate spheroid in xyz coordinates, (b) oblate spheroid projected into y-z plane showing ξ and θ at different values; φ is the angle of rotation around the z axis (adopted from Happel and Brenner [27]).

where f is the focal length, $f = \sqrt{a^2 - b^2}$, a and b are the semi-major axis and the semi-minor axis of the ellipse respectively. According to Eq. (1), spheroid's surface with $\xi = \text{constant}$ can be represented by:

$$\left(\frac{1}{f^2 \cosh^2 \xi}\right) X^2 + \left(\frac{1}{f^2 \cosh^2 \xi}\right) Y^2 + \left(\frac{1}{f^2 \sinh^2 \xi}\right) Z^2 = 1 \quad (2)$$

Eq. (2) generates a family of oblate spheroids having their geometric center at the origin. In oblate spheroidal coordinate system, ξ , θ and φ are used describe spheroids in three-dimensional space, ξ coordinate has two limiting values, $\xi = 0$, which represents a disk-like shape and as ξ increases, ellipses of various sizes are generated, as $\xi \rightarrow \infty$ a sphere is formed. The θ coordinate is the angular coordinate and describes a system of hyperbolas, and vary in the range $[0, \pi]$. The φ coordinate, is the longitudinal (azimuthal) angle and vary in the range $[0, 2\pi]$.

The oblate spheroidal coordinates' metric coefficients are given by

$$h_\xi = h_\theta = \frac{1}{f \cdot \sqrt{\cosh^2 \xi - \sin^2 \theta}}, h_\varphi = \frac{1}{f \cdot \cosh \xi \cdot \sin \theta} \quad (3)$$

These metric coefficient are used to transform the governing equations from rectangular coordinates into oblate spheroidal coordinate system [27].

The energy conservation in 3D orthogonal coordinates can be written as [29]

$$\frac{\partial T}{\partial t} = \alpha \cdot h_\xi h_\theta h_\varphi \left[\frac{\partial}{\partial \xi} \left(\frac{h_\theta h_\varphi}{h_\xi} \frac{\partial T}{\partial \xi} \right) + \frac{\partial}{\partial \theta} \left(\frac{h_\xi h_\varphi}{h_\theta} \frac{\partial T}{\partial \theta} \right) + \frac{\partial}{\partial \varphi} \left(\frac{h_\xi h_\theta}{h_\varphi} \frac{\partial T}{\partial \varphi} \right) \right] \quad (4)$$

The metric coefficients for oblate spheroid defined in Eq. (3) are used to transform Eq. (4) into oblate coordinate system. The third term in RHS of Eq. (4) is neglected (φ coordinate) because of its rotational symmetry around z axis. In two-dimensional oblate orthogonal coordinate system, Eq. (4) then takes the form

$$\frac{\partial T}{\partial t} = \frac{\alpha}{f^2 (\cosh^2 \xi - \sin^2 \theta)} \left[\tanh \xi \cdot \frac{\partial T}{\partial \xi} + \frac{\partial^2 T}{\partial \xi^2} + \cot \theta \cdot \frac{\partial T}{\partial \theta} + \frac{\partial^2 T}{\partial \theta^2} \right] \quad (5)$$

where α is the thermal diffusivity of the droplet $\alpha = \frac{k_d}{\rho_d \cdot c_p}$.

Two-dimensional (2D) axisymmetric computational model for the oblate droplets is assumed (see Fig. 2), the grid system is used to solve the PDE heat equation (Eq. (5)), the initial and boundary conditions are

$$T = T_0, \text{ at } t = 0, \frac{\partial T}{\partial \theta} = 0, \text{ at } \theta = 0 \text{ and } \theta = \pi, \frac{\partial T}{\partial \xi} = 0, \text{ at } \xi = 0 \quad (6)$$

The boundary condition at the spheroid surface, $\xi = \xi_s$ reads as

$$k_d(\theta) \frac{1}{f \cdot \sqrt{\cosh^2 \xi - \sin^2 \theta}} \frac{\partial T}{\partial \xi} = h_g(\theta)(T_{air} - T(\theta)) + \lambda(\theta) \frac{\dot{m}_{eva}(\theta)}{A_{os}} \quad (7)$$

Eq. (7) represents the coupling between the liquid phase (droplet surface) and the gas phase in terms of energy transfer. A_{os} is the surface area of oblate droplet. The heat transfer coefficient is calculated from local Nusselt number, $h_g = Nu(\theta) \frac{k_d(\theta)}{L_c}$. $Nu(\theta)$ takes

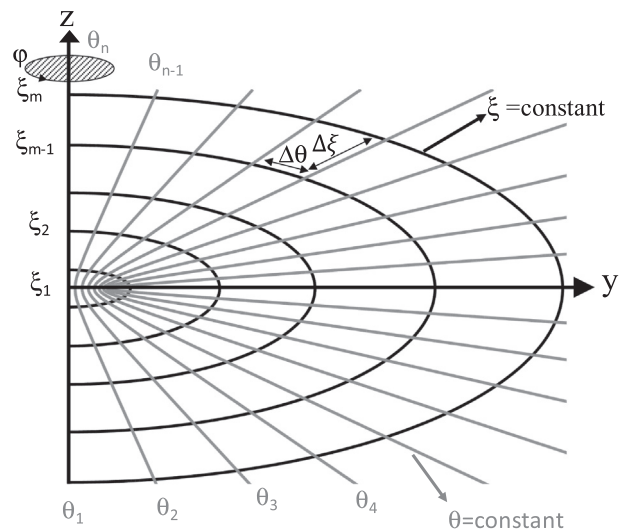


Fig. 2. 2-D grid system of an oblate droplet; the grid system used to solve Eqs. (5)–(8).

the same form as Eq. (12) by replacing \mathfrak{D}_g with thermal diffusivity, α . The heat transfer coefficient is calculated at each grid point on droplet surface.

The local rate of liquid evaporation from the droplet surface is determined by the following

$$\dot{m}(\theta)_{eva} = \rho_g \mathfrak{D}_g \frac{A_{os}}{L_c} \cdot Sh(\theta) \cdot \frac{y_{vap,s}(\theta) - y_{vap,\infty}}{1 - y_{vap,s}(\theta)} \quad (8)$$

where L_c is the characteristic length, for a spherical droplet, L_c is the droplet diameter, $L_c = 2a$ for an oblate droplet.

The mass fraction of the vapor at the droplet surface is defined as follows

$$y_{vap,s} = \left[1 + \left(\frac{P_{amt}}{P_{vap,s}^*(T_s)} - 1 \right) \cdot \frac{Mw_{air}}{Mw_{vap}} \right]^{-1} \quad (9)$$

where $P_{vap,s}^*(T_s)$ is the vapor pressure at the droplet's surface temperature T_s and P_{amt} is the ambient gas pressure, the vapor concentration far away from droplet surface, namely, outside the outer acoustic boundary layer, $y_{vap,\infty} = 0$.

The surface area A_{os} and the volume of an oblate droplet are defined as follows

$$A_{os} = 2\pi a^2 \left(1 + \frac{1 - e^2}{2e} \ln \left(\frac{1 + e}{1 - e} \right) \right) \quad (10)$$

$$V_{os} = \frac{1}{6} \pi \cdot A_R \cdot L_{major}^3 \quad (11)$$

where e is the oblate spheroid eccentricity. A_R is the Aspect ratio of the spheroid, $A_R = b/a$. For an oblate spheroid, A_R takes values between $0 < A_R < 1$, in case of a spherical droplet, $a = b$ and A_{os} in Eq. (10) can be easily shown to be equal to $4\pi a^2$.

The 2-D heat equation (Eq. (5)) was numerically solved using a numerical scheme called Alternating Direction Implicit (ADI) method [30], the ADI method is unconditionally stable with truncating error of 2nd order in time and spatial coordinates, step size used in ξ and θ coordinates was calculated for 50 and 61 nodal points respectively and a time step of 0.1 s.

The model presented in this section overlaps with the evaporation model developed by a recent work from our laboratory [23] in terms of the geometrical coordinate system used. However, the mass/heat transfer parameters in this work are related to the acoustic boundary layer. Gopinath and Mills [31] studied experimentally and numerically the convective heat transfer from an isolated spherical particle in the acoustic field by solving the governing equations of energy and flow dynamics. Mass and heat transfer correlations in terms of Sh/Nu numbers were developed for liquid droplet evaporation induced by the inner acoustic streaming [32], the equation of the local Sh number over the droplet surface reads as

$$Sh(\theta) = 2 \cdot K_{acoustic} \frac{B}{(\omega \mathfrak{D}_g)^{1/2}} \frac{\cos^2 \theta}{(1 + \cos^2 \theta)^{1/2}} \quad (12)$$

where B is a velocity scale of the incident sound wave that depends on the sound pressure amplitude A_{0e} , $B = A_{0e}/(\rho_g c_s)$, ω is the angular frequency of the incident sound wave. $K_{acoustic}$ is a dimensionless factor, its value depends mainly on liquid properties, drop volume, shape and properties of the incident acoustic wave. For small spherical droplets it takes an asymptotic value of 1.89 and for an oblate droplets, $K_{acoustic}$ varies in the range of 2–3 [32]. The sound pressure level (SPL) for pure liquid droplet can be estimated by measuring the intensity of the incident sound wave by using a reflector equipped with piezoelectric sensor. For pure liquids, Yarin et al. [33] developed a numerical method (YPT) to calculate the SPL, its

value depends on aspect ratio, volume and surface tension of the droplet.

$$SPL = 20 \log_{10} A_{0e} + 74 \quad (13)$$

3. Experimental method

Many researchers have used the ultrasound field to study heat and mass transfer from a small solid particle or a liquid droplet [7,34–42]. Chainani and coworkers [43,44] developed a lab-on-chip deployment of acoustic levitation to investigate reactions at the microliter scale. The levitated droplet can be considered as a microreactor. In acoustic levitation, the mechanical intrusion is eliminated; the force balance between the acoustic force and the droplet weight help suspend the droplet in the air.

The acoustic force is formed by the standing acoustic wave; droplets of a few millimeters down to 100 μm can be levitated. This makes the acoustic levitator useful in many fundamental investigations related to spray and droplet generation and maintaining the droplet under well-defined process parameters.

As shown in Fig. 3, the acoustic levitator consists of the concave reflector aligned axially with a transducer flange integrated with an oscillating piezocrystal at 58 kHz. The distance between the transducer and the reflector is adjusted via a micrometer screw.

The acoustic waves emitted from the transducer travel through the gas medium and hit the reflector. Then they bounce back to the transducer forming the so-called standing wave. The distance between the reflector and the transducer is a multiple of half-wavelengths. The acoustic radiation pressure exerted on the droplet is measured in terms of the sound pressure level (SPL, dB). The intensity of the acoustic force is tuned by changing the driving voltage of the piezocrystal; the acoustic force counteract the gravity force and, thus, droplet can be levitated.

The droplet is monitored online by a CMOS camera (1280 × 1024) with up to 200 fps; a macro lens is attached to the camera to obtain better magnification and focus on the droplet. The droplet is illuminated from behind by a white LED light source. The camera captures a shadow image of the droplet during evaporation at predefined rate of 1 Hz. In-house-developed image processing software was used to analyze these high-quality images. Based on these images, the evaporation rate of the droplet was calculated by determining the major and minor axes, the surface area and the position in the acoustic field. The measurement of droplet size from the meridional contour via shadow imaging technique is calibrated by levitating a small glass sphere of known diameter at different back light intensity, length uncertainty of $\pm 5 \mu\text{m}$ is obtained. The droplet with the desired volume is inserted into the acoustic

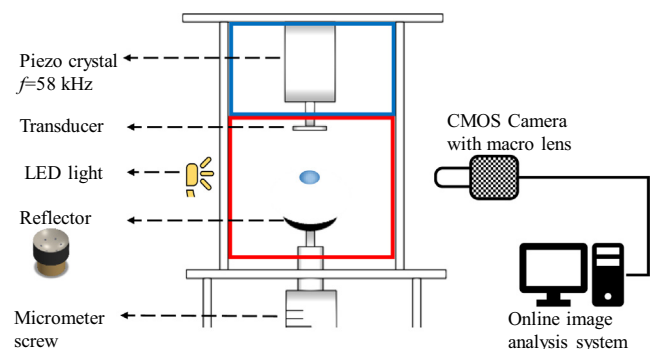


Fig. 3. The experimental setup used to measure the evaporation rate of oblate spheroid droplets; it consists mainly of the acoustic levitator (tec5 AG Sensorik und Systemtechnik) and an image acquisition system; CMOS Camera (MQ013xG-ON, XIMEA GmbH) and macro lens (Navitar Zoom 6000).

field via a concentric hole in the transducer with a microliter syringe, the liquid is pressed through the needle to deliver the droplet into desired position i.e., pressure node, the syringe has an overall volume of 5 μl with an accuracy of $\pm 0.05 \mu\text{l}$.

4. Acoustic streaming and air ventilation experiments

The interaction between a levitated droplet and the acoustic standing wave generates a streaming flow around the droplet [45,46], the acoustic streaming is divided into two types; the inner acoustic streaming adjacent to the droplet surface, which influence the mass and heat transfer rate at the droplet's surface through the convective acoustic boundary layer [32,42]. The second type is the outer acoustic streaming that consists of four outer toroidal vortices surrounding the droplet [31,42]. The presence of these toroidal vortices has an artifact on the evaporation of liquid droplets, vapor is trapped in these closed zones. Further accumulation of the vapor changes the temporal vapor concentration in the far field from the droplet surface.

Therefore, it's important to blow out these vortices by an external flow either axial [42,45,47] or normal to the axis of levitation [32], in any case, the ventilation should be strong enough to deplete the vapor without disturbing the inner acoustic boundary layer. A plateau ventilation curve of the blowing air flow would be used to set the optimal blowing flow rate of the air, a ventilation curve as presented in Fig. 4, is used to determine the optimal ventilation air flow rate. The evaporation rate constant (β) is calculated from temporal evolution of the equatorial diameter L_{major}^2 . The drop evaporation was measured as a function of air flow rate. It can be seen from Fig. 4, the air ventilation affects the evaporation, note that, at very small ventilation rates ($< 0.6 \text{ l/min}$), droplet evaporation is hindered due to the accumulation of the vapor in the outer vortices. As the ventilation flow rate increases, the evaporation increases until it reaches a constant evaporation rate ($0.6\text{--}1.1 \text{ l/min}$). Further increase of flow rate leads to unstable droplet levitation and air flow begins to disturb the inner acoustic streaming. In the experimental setup, the air is inserted beneath the droplet from the concave reflector, which has an array of six holes (see Fig. 3) that allow the air coming out to surround the droplet. Such ventilation is mandatory to prevent the accumulation of vapor; otherwise, the assumption ($\gamma_{\text{vap},\infty} = 0$) in the computational model does not hold.

5. Evaporation of spheroidal droplet at fixed aspect ratio

The acoustic radiation pressure exerted on the droplet generates an acoustic force acting upwards, if the acoustic force is strong enough to compensate for the droplet weight, levitation is possible; in this case, the droplet is located in a position slightly below a pressure node.

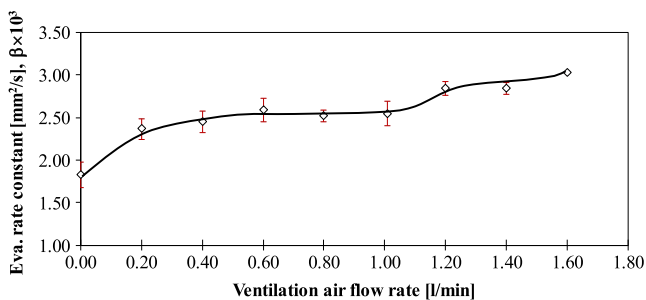


Fig. 4. Ventilation curve of the toroidal vortices at different air flow rates. Evaporation rate constant (β) plotted versus the air flow rate. Experiments of water evaporation conducted at ambient dry air temperature of 22°C .

Due to the non-uniformity of the acoustic radiation, the droplet takes an oblate shape. At a constant acoustic radiation pressure amplitude, further increase of the droplet's volume will force the droplet to fall due to the gravity force. In the present study, experiments were conducted with levitated droplets at a constant aspect ratio. First, liquid droplets were inserted via a microliter syringe into the acoustic field. Then the sound pressure level was adjusted so the acoustic force deforms the droplet shape into a desired aspect ratio of ($b/a \approx 0.7$). This aspect ratio was selected in such a way that it could be realized in the acoustic levitator. On the other hand, it also showed an apparent deviation in shape compared to a spherical droplet. The intensity of the acoustic force, the volume of the levitated droplet and its surface tension play a role in determining droplet shape. For large volumes, the surface tension forces become smaller; the applied acoustic force can squeeze the droplet to the desired aspect ratio.

As the droplet evaporates, its volume becomes smaller and the surface tension forces become greater, forcing the droplet shape to approach an equilibrium geometry, e.g., a spherical shape [48,49].

The evaporation of pure methanol, toluene and heptane liquids were investigated; the physical properties of these liquids are listed in Table 1. An initial droplet volume of $2.5 \mu\text{l}$ was levitated in the acoustic field. The shadowgraphy technique and image analysis system implemented for the experiments allowed an online analysis of the meridional shape of the droplet i.e., the major and minor axes were calculated. As shown in Fig. 5, the aspect ratio during the evaporation experiment was kept at almost 0.71 ± 0.03 . A larger deviation from the desired aspect ratio occurred at the first few seconds of the evaporation during the adjustment of the acoustic force. The droplet aspect ratio was successfully kept constant for an evaporation time of approximately $80\text{--}100 \text{ s}$. As the droplet volume decreases the applied acoustic force is no longer capable of squeezing the droplet to the desired aspect ratio, the aspect ratio then begins to increase steadily approaching spherical shape.

Table 1
Physical properties of investigated liquids, at an ambient temperature of 22°C .

	Density [kg/m^3]	Surface tension [mN/m]	Diffusion coefficient [m^2/s]	Vapor pressure [kPa]
Heptane	684.0	20.1	6.735×10^{-6}	5.242
Methanol	790.5	22.7	15.89×10^{-6}	14.41
Toluene	867.0	28.4	7.354×10^{-6}	3.226

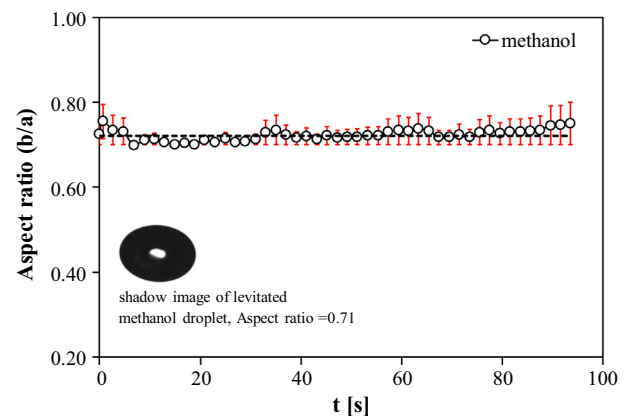


Fig. 5. Temporal evolution of aspect ratio (b/a) for methanol liquid. The droplet was held in the acoustic field at an almost steady aspect ratio of 0.71 ± 0.03 during the course of evaporation, the dashed line represents the aspect ratio of 0.71.

The temporal evolution of the major axis versus dimensionless time is shown in Fig. 6. The change in normalized surface decay ($L_{major}^2/L_{major,0}^2$) is depicted for all three liquids. Measurements were repeated in triplets for each liquid, all experimental data show a high repeatability. The equatorial droplet diameter (L_{major}) indicates an average value. The error bars are the standard error ($SE = \frac{\sigma}{\sqrt{n}}$) of the measured values and represent the uncertainty. The evaporation curves follow a linear trend with a negative slope. It can be stated that the evaporation corresponds to the so-called d^2 -law ($L_{major}^2(t)$ is linear). These results show that the evaporation of oblate droplets is similar to the acoustically driven evaporation of spherical droplets [42].

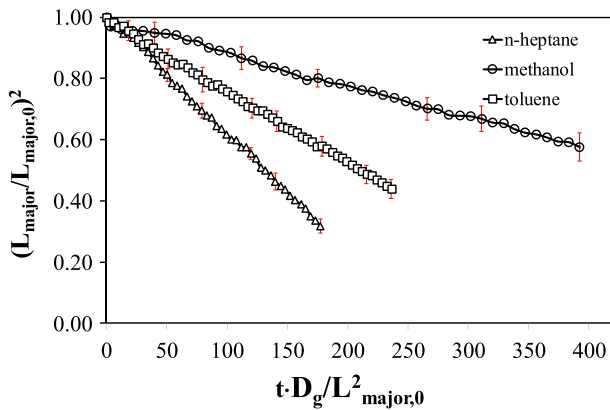


Fig. 6. The squared major axis of the oblate droplet rendered by the initial major axis versus dimensionless time for (a) n-heptane, (b) methanol and (c) toluene; experiments were carried out at 22 °C ambient gas temperature and 1% relative humidity.

6. Model validation and comparison

The evaporation model developed for an acoustic driven evaporation of deformed liquid droplets is validated and discussed in this section. Droplet physico-chemical properties of liquid droplet are calculated at each grid point and are updated at each time step. The calculated local rate of droplet evaporation is averaged over droplet surface and used to calculate the droplet equatorial diameter $L_{major}(t)$ [23].

The value of $L_{major}^2/L_{major,0}^2$ represents the surface decay of the oblate droplet rendered by its initial surface area (see Eq. (10)). The term between brackets in the RHS of Eq. (10) is a shape factor and remains constant during evaporation, its value depends solely on the droplet’s aspect ratio (A_R).

The theoretical model in oblate spheroidal coordinates (Eqs. (5)-(8)) predicts the evaporation of an oblate spheroid at a constant aspect ratio. The vapor concentration ($y_{vap,\infty}$) outside the acoustic boundary layer is assumed in the model to be $y_{vap,\infty} = 0$; therefore, a blowing of the outer acoustic streaming is imposed inside the levitator around the droplet as demonstrated in Fig. 4.

The computational model was compared with experiments of each liquid as shown in Fig. 7. The experimental results are in a good agreement with model prediction. It can be seen from Fig. 7a that model prediction for n-heptane deviates slightly from experimental values. Once the droplet is inserted into the acoustic field, some time is required to adjust the droplet shape and to stabilize the droplet, and thus it takes few seconds until recording of the droplet shadow image is initiated. The droplet in the experiment had already then approached its equilibrium temperature which is less than the initial liquid temperature.

The model predicts the evaporation starting from $t = 0$ and an initial temperature of 22 °C, the model calculates the equilibrium temperature from the thermal balance. Therefore, the droplet experience faster evaporation at the beginning until it reaches the surface equilibrium temperature.

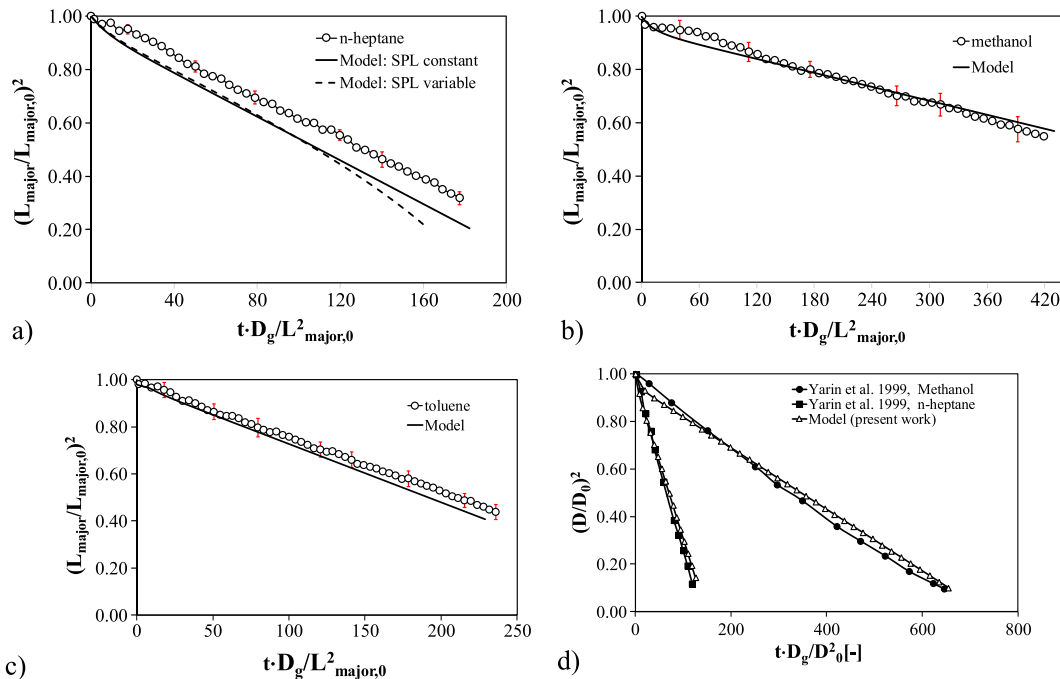


Fig. 7. Experimental results compared to the theoretical model; the surface area of spheroids is rendered by its initial surface area. (a) n-heptane, (b) methanol (c) toluene and (d) methanol and n-heptane experiments from Yarin et al. [32] work. Experiments conducted at ambient dry air temperature of 22 °C. The abscissa is a non-dimensional time i.e. evaporation time rendered by characteristic diffusion time.

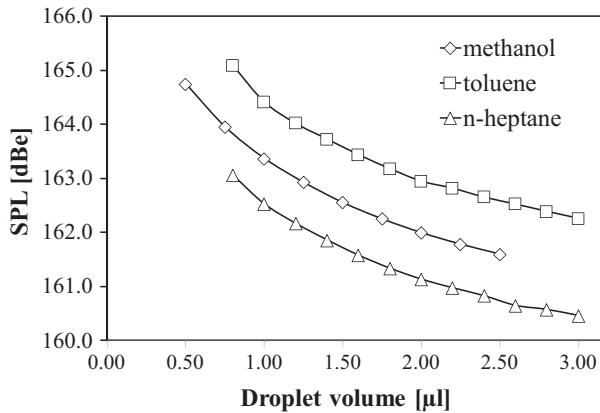


Fig. 8. Sound pressure level (SPL) in dB calculated for methanol, n-heptane and toluene for different droplet volumes at a constant aspect ratio ($A_R = 0.7$).

Evaporation of both methanol and n-heptane in the acoustic levitator were also conducted by Yarin et al. [32] and are depicted in Fig. 7d. The evaporation experiments begin with an initial volume of $3.0 \mu\text{l}$ and an initial aspect ratio of $a/b = 1.8$ (Fig. 8, [32]), this is actually equivalent to an aspect ratio of $b/a = 0.55$ (notation used in current work). In their work [32], no active control of the acoustic force was applied, therefore, the axis ratio of the drop is changing during the evaporation process until it approaches unity (perfect sphere). Note that, experiments of methanol and n-heptane were performed in this work at constant aspect ratio of approximately 0.7 during the process of evaporation. As shown in Fig. 7d, the computational 2D evaporation model succeeded to predict the course of evaporation of both liquids studied by Yarin et al. [32].

The timed-average local Sh number is calculated from Eq. (12). The Sh number takes a maximum value near the equator of the droplet, where the mass and heat transfer are their maximum

[32,50]. The model calculates the evaporation for an oblate spheroid of a 0.7 aspect ratio. In these simulation results, the SPL was calculated for the droplet at the beginning of evaporation. Droplet volume, oblateness and liquid surface tension influence SPL values. At aspect ratio ($A_R = 0.7$), the sound pressure level was calculated for droplets at different volumes using the YPT method [33].

As shown in Fig. 8, as the droplet's volume decreases, higher SPL values are required to levitate droplets at an aspect ratio of 0.7. A variable SPL during evaporation was modeled for n-heptane (see Fig. 7a). One can see that at $t > 100$ s, the evaporation rate calculated with the variable SPL becomes faster (dotted curve). SPL becomes larger at a smaller droplet volume; thus, evaporation rate increases.

7. Influence of droplet oblateness on evaporation rate

In the present section, the influence of droplet oblateness on evaporation behavior is analyzed. In modelling the evaporation of liquid droplets at other aspect ratios, the initial droplet volume was assumed to be the same in all computation trials, and the equatorial diameter, $L_{\text{major},0}$ was then calculated for each aspect ratio from the volume of an oblate spheroid, (see Eq. (11)), these modelling trials corresponds to volume-equivalent spheroid evaporation [23].

The evaporation of toluene droplet at varying aspect ratio is displayed in Fig. 9. The normalized surface curves in Fig. 9a show that the smaller the aspect ratio, the faster the surface area decay of the droplet i.e., evaporation is enhanced. The surface area of a droplet of the same equivalent volume increases as the aspect ratio decreases. Deformed droplet in strong acoustic field requires larger acoustic pressure to achieve the desired oblateness at smaller aspect ratio, thus mass transfer parameter in terms of Sh number will increase (see Eq. (12)).

Fig. 9b shows the evaporation rate ($|\dot{m}|_{\text{eva}}$) averaged over droplet surface, the curves exhibit the presence of two different slopes, the first regime ends when the droplet temperature reached its

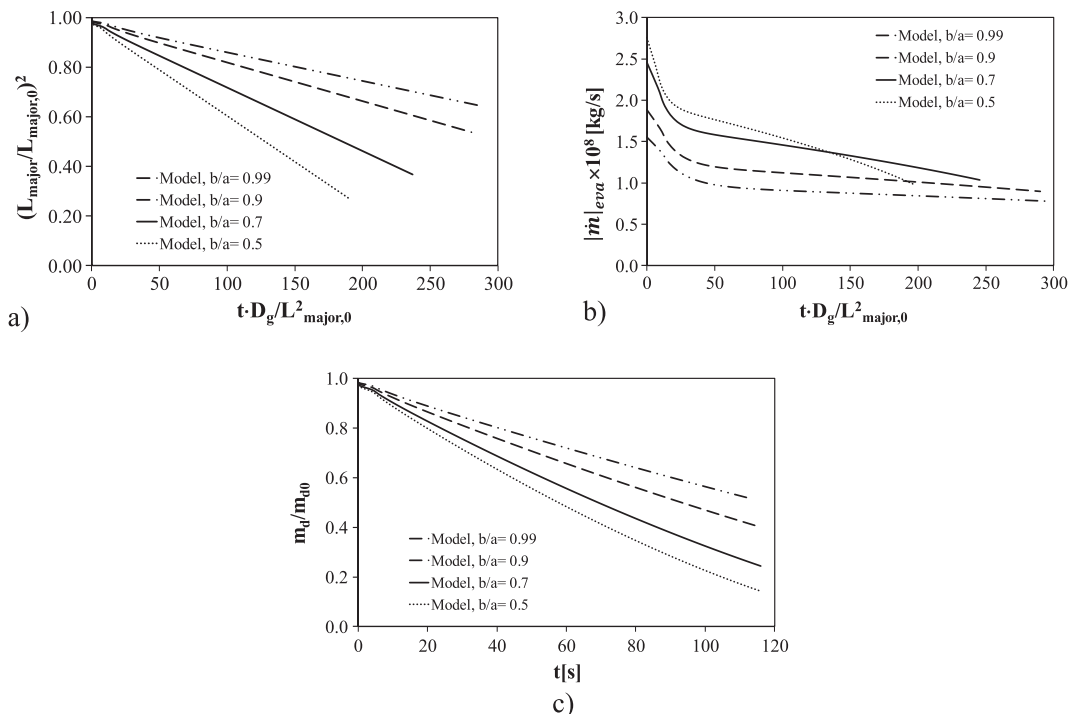


Fig. 9. Modeling of toluene droplet evaporation at 22°C and an initial volume of $2.5 \mu\text{l}$ (a) influence of aspect ratio on the evolution of normalized surface decay of toluene droplet, (b) evolution of evaporation rate and (c) temporal evolution of droplet mass rendered dimensionless by its initial mass.

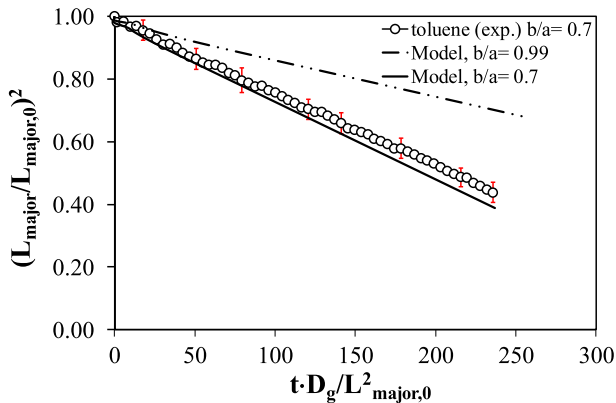


Fig. 10. Comparison of the evaporation of toluene droplet at an aspect ratio of 0.7 and model predictions for aspect ratio ($A_R = 0.7$ and $A_R = 0.99$). Results show the bias that might occur when modelling the droplet using the spherical geometry model instead of an oblate spheroidal model.

equilibrium temperature i.e., dew point temperature, the first regime takes about 8–10 s. As the deformation of droplet increase the evaporation rate increases as well, it can be seen at $A_R = 0.5$, the slope of the evaporation rate curve is significantly larger than other aspect ratios, therefore, the evaporated mass is larger. It can be seen from Fig. 9c that more than 75% of droplet mass was evaporated for an aspect ratio of 0.5 after 100 s is elapsed, while only 45% of droplet liquid was evaporated for an aspect ratio of 0.99.

The simulation of an almost spherical droplet of an aspect ratio of 0.99 is shown in Fig. 10. The droplet here corresponds to an almost perfect sphere. One can see that the spherical droplet evaporates slower compared to a deformed droplet. Fig. 10 shows the deviation of a model prediction that might occur from experimental results if the sphericity shape factor of the oblate droplet is neglected and the droplet is modeled by the spherical geometry model.

8. Conclusions

A theoretical and experimental study for the evaporation of acoustically levitated oblate liquid droplet is conducted. The evaporation rate of an oblate liquid droplet driven by an acoustic field was measured experimentally for n-heptane, methanol and toluene. The experiments were carried out under a constant aspect ratio and the intensity of the acoustic field was adjusted continuously to keep the droplet shape at an aspect ratio of 0.7 approximately during the evaporation. The experimental results revealed that evaporation of spheroidal droplets followed the well-known d^2 -law.

A computational model to describe the evaporation was presented. The droplet shape is described as an oblate spheroid with rotational symmetry around z-axis. The predicted evaporation rate fits well with experimental data, indicating that model has successfully captured the influence of geometrical deformation on droplet evaporation.

Simulation trials shows that by decreasing aspect ratio, the evaporation rate become faster. The deviation between experimental results for oblate droplet evaporation and model predictions (if spherical geometry is assumed) reveals the need to consider model implementation using an oblate spheroidal coordinate system.

The experimental technique used to study the evaporation of a freely suspended oblate spheroid droplet at a pre-defined droplet geometry allows for the validation of the theoretical model in the oblate coordinate system, which is rather difficult to achieve experimentally for liquid droplets in sprays.

Conflict of interest

The author declared that there is no conflict of interest.

Acknowledgements

This work was supported by the Deanship of Scientific Research (DSR), King Abdulaziz University, Jeddah, under grant No. (D076-135-1439). The author, therefore, gratefully acknowledge the DSR technical and financial support.

References

- [1] N.A. Fuchs, *Evaporation and Droplet Growth in Gaseous Media*, Pergamon Press, London, 1959.
- [2] R.B. Bird, W.E. Stewart, E.N. Lightfoot, *Transport Phenomena*, Wiley International Edition, New York, 1960.
- [3] W.E. Ranz, W.R. Marshall, *Evaporation from drops Part I and II*, Chem. Eng. Progr. 48 (1952).
- [4] N. Frössling, *On the evaporation of falling drops*, Gerl. Beitr Geophys. 52 (1938) 170–216.
- [5] B. Abramzon, W.A. Sirignano, *Droplet vaporization model for spray combustion calculations*, Int. J. Heat Mass Transfer 32 (9) (1989) 1605–1618.
- [6] G. Yao, *A film-theory-based model for a multicomponent droplet evaporation at both low- and high-pressure environments*, J. Heat Transfer 128 (2006) 290–294.
- [7] G. Brenn, L.J. Deviprasath, F. Durst, C. Fink, *Evaporation of acoustically levitated multi-component liquid droplets*, Int. J. Heat Mass Transfer 50 (25) (2007) 5073–5086.
- [8] N.E. Rawson, J.S. Chinn, W.F. Stevens, *Computer calculation of binary- drop evaporation*, AIChE J. 7 (3) (1969) 448–452.
- [9] M. Burger, R. Schmehl, K. Prommersberger, O. Schäfer, R. Koch, S. Wittig, *Droplet evaporation modeling by the distillation curve model: accounting for kerosene fuel and elevated pressures*, Int. J. Heat Mass Transfer 46 (23) (2003) 4403–4412.
- [10] M. Renksibulut, M. Bussmann, X. Li, *A droplet vaporization model for spray calculations, Part. Part. Syst. Charact.* 9 (October 1991) (1992) 59–65.
- [11] M. Burger, G. Klose, *A combined eulerian and lagrangian method for prediction of evaporating sprays*, J. Eng. Gas Turb. Power 124 (2002) 481–488.
- [12] M. Birouk, S.C. Fabbro, *Droplet evaporation in a turbulent atmosphere at elevated pressure – experimental data*, Proc. Combust. Inst. 34 (1) (2013) 1577–1584.
- [13] F. Mashayek, *Dynamics of evaporating drops. Part I: formulation and evaporation model*, Int. J. Heat Mass Transf. 44 (2001) 1517–1526.
- [14] E. Loth, *Quasi-steady shape and drag of deformable bubbles and drops*, Int. J. Multiph. Flow 34 (6) (2008) 523–546.
- [15] M. Dai, J.B. Perot, D.P. Schmidt, *Heat transfer within deforming droplets*, Proc. ASME 1 (2002) 1–6.
- [16] G. Juncu, *Unsteady heat transfer from an oblate/prolate spheroid*, Int. J. Heat Mass Transf. 53 (17–18) (2010) 3483–3494.
- [17] N. Kishore, S. Gu, *Momentum and heat transfer phenomena of spheroid particles at moderate Reynolds and Prandtl numbers*, Int. J. Heat Mass Transf. 54 (11–12) (2011) 2595–2601.
- [18] R. Alassar, M. Abushosha, M. El-Gebeily, *Transient heat conduction from spheroids*, Trans. Can. Soc. Mech. Eng. 38 (3) (2014) 373–389.
- [19] B. Srinivas, K.V. Ramesh, *Numerical analysis of heat transfer from a spheroidal shaped body to a power law fluid at finite Reynolds number*, CFD Lett. 6 (1) (2014) 1–14.
- [20] S. Tonini, G.E. Cossali, *An evaporation model for oscillating spheroidal drops*, Int. Commun. Heat Mass Transfer 51 (2014) 18–24.
- [21] S. Tonini, G.E. Cossali, *One-dimensional analytical approach to modelling evaporation and heating of deformed drops*, Int. J. Heat Mass Transfer 97 (2016) 301–307.
- [22] J. Li, J. Zhang, *A theoretical study of the spheroidal droplet evaporation in forced convection*, Phys. Lett. A 378 (47) (2014) 3537–3543.
- [23] B. Al Zaitone, *Evaporation of oblate spheroidal droplets: a theoretical analysis*, Chem. Eng. Commun. 205 (1) (2018) 110–121.
- [24] R. Clift, J.R. Grace, M.E. Weber, *Bubbles, Drops and Particles*, Academic Press, New York, 1978.
- [25] M.M.R. Williams, *Thermophoretic forces acting on a spheroid*, J. Phys. D Appl. Phys. 19 (9) (1986) 1631.
- [26] J. Chen, N.E. Clay, P. No-hyung, H. Kong, *Non-spherical particles for targeted drug delivery*, Chem. Eng. Sci. 125 (2015) 20–24.
- [27] J. Happel, H. Brenner, *Low Reynolds Number Hydrodynamics*, Martinus Nijhoff, The Hague, The Netherlands, 1983.
- [28] P. Moon, D.E. Spencer, *Field Theory Handbook, second ed.*, Springer-Verlag Berlin, Heidelberg, 1971.
- [29] M.N. Ozisik, *Finite Difference Methods in Heat Transfer*, John Wiley & Sons, New York, 1993.
- [30] J.J. Douglas, J.E. Gunn, *A general formulation of alternating direction methods. Part I: parabolic and hyperbolic problems*, Numer. Math. 6 (1964) 428–453.

- [31] A. Gopinath, A.F. Mills, Convective heat transfer from a sphere due to acoustic streaming, *J. Heat Transfer* 115 (2) (1993) 332–341.
- [32] A.I. Yarin, G. Brenn, O. Kastner, D. Rensink, C. Tropea, Evaporation of acoustically levitated droplets, *Fluid Mech.* 399 (1999) 151–204.
- [33] A.I. Yarin, M. Pfaffenlehner, C. Tropea, On the acoustic levitation of droplets, *Fluid Mech.* 356 (1998) 65–91.
- [34] T. Furuta, M. Okazaki, R. Toei, E.J. Crosby, Formation of crystals on the surface of Non-supported droplet in drying, in: A.S. Mujumdar (Ed.), *International Drying Symposium*, Hemisphere-McGraw-Hill, New York, 1982, pp. 157–164.
- [35] C. Moeser, C. Groenewold, H. Groenewold, E. Tsotsas, Untersuchung der kinetik von trennprozessen im akustischen levitator: vor- und nachteile, *Chem. Ing. Tech.* 73 (2001) 1012–1017.
- [36] R. Tuckermann, S. Bauerecker, B. Neidhart, Evaporation rates of alkanes and alkanols from acoustically levitated drops, *Anal. Bioanal. Chem.* 372 (1) (2002) 122–127.
- [37] R. Mondragon, L. Hernandez, J.E. Julia, J.C. Jarque, S. Chiva, B. Zaitone, C. Tropea, Study of the drying behavior of high load multiphase droplets in an acoustic levitator at high temperature conditions, *Chem. Eng. Sci.* 66 (12) (2011) 2734–2744.
- [38] Z. Chen, D. Zang, L. Zhao, M. Qu, X. Li, X. Li, L. Li, X. Geng, Liquid marble coalescence and triggered microreaction driven by acoustic levitation, *Langmuir* 33 (25) (2017) 6232–6239.
- [39] N.A. Combe, D.J. Donaldson, Water evaporation from acoustically levitated aqueous solution droplets, *J. Phys. Chem. A* 121 (38) (2017) 7197–7204.
- [40] B. Al Zaitone, A. Lamprecht, Single droplet drying step characterization in microsphere preparation, *Colloids Surf. B-Biointerfaces* 105 (2013) 328–334.
- [41] O. Kastner, G. Brenn, D. Rensink, C. Tropea, The acoustic tube levitator: a novel device for determining the drying kinetics of single droplets, *Chem. Eng. Technol.* 24 (4) (2001) 335–339.
- [42] B.A. Al Zaitone, C. Tropea, Evaporation of pure liquid droplets: Comparison of droplet evaporation in an acoustic field versus glass-filament, *Chem. Eng. Sci.* 66 (17) (2011) 3914–3921.
- [43] E.T. Chainani, W.-H. Choi, K.T. Ngo, A. Scheeline, Mixing in colliding, ultrasonically levitated drops, *Anal. Chem.* 86 (4) (2014) 2229–2237.
- [44] E.T. Chainani, K.T. Ngo, A. Scheeline, Electrochemistry in an acoustically levitated drop, *Anal. Chem.* 85 (4) (2013) 2500–2506.
- [45] E.H. Trinh, J.L. Robey, Experimental study of streaming flows associated with ultrasonic levitators, *Phys. Fluids* 6 (11) (1994) 3567–3579.
- [46] K. Hasegawa, Y. Abe, A. Kaneko, Y. Yamamoto, K. Aoki, Visualization measurement of streaming flows associated with a single-acoustic levitator, *Micrograv. Sci. Technol.* 21 (Suppl. 1) (2009) 9–14.
- [47] A.I. Yarin, G. Brenn, J. Keller, M. Pfaffenlehner, E. Ryszel, C. Tropea, Flowfield characteristics of an aerodynamic acoustic levitator, *Am. Inst. Phys.* 9 (11) (1997).
- [48] Y. Tian, R.G. Holt, R.E. Apfel, Deformation and location of an acoustically levitated liquid drop, *J. Acoust. Soc. Am.* 93 (6) (1993) 3096–3104.
- [49] H.E. Trinh, C.-J. Hsu, Equilibrium shapes of acoustically levitated drops, *J. Acoust. Soc. Am.* 79 (5) (1986) 1335–1338.
- [50] N. Kawahara, A.L. Yarin, G. Brenn, O. Kastner, F. Durst, Effect of acoustic streaming on the mass transfer from a sublimating sphere, *Phys. Fluids* 12 (4) (2000).